Available online at www.sciencedirect.com
ScienceDirect
Geochimica et Cosmochimica Acta 73 (2009) 4423–4436
Geochimica et Cosmochimica Acta
www.elsevier.com/locate/gca

A surface structural model for ferrihydrite I: Sites related to primary charge, molar mass, and mass density

Tjisse Hiemstra *, Willem H. Van Riemsdijk

Department of Soil Quality, Wageningen University, P.O. Box 47, 6700 AA Wageningen, The Netherlands

Received 9 December 2008; accepted in revised form 28 April 2009; available online 12 May 2009

Abstract

A multisite surface complexation (MUSIC) model for ferrihydrite (Fh) has been developed. The surface structure and composition of Fh nanoparticles are described in relation to ion binding and surface charge development. The site densities of the various reactive surface groups, the molar mass, the mass density, the specific surface area, and the particle size are quantified. As derived theoretically, molecular mass and mass density of nanoparticles will depend on the types of surface groups and the corresponding site densities and will vary with particle size and surface area because of a relatively large contribution of the surface groups in comparison to the mineral core of nanoparticles. The nano-sized (~2.6 nm) particles of freshly prepared 2-line Fh as a whole have an increased molar mass of $M \sim 101 \pm 2$ g/mol Fe, a reduced mass density of $\sim 3.5 \pm 0.1$ g/cm^3, both relatively to the mineral core. The specific surface area is ~ 650 m^2/g. Six-line Fh (5–6 nm) has a molar mass of $M \sim 94 \pm 2$ g/mol, a mass density of $\sim 3.9 \pm 0.1$ g/cm^3, and a surface area of $\sim 280 \pm 30$ m^2/g. Data analysis shows that the mineral core of Fh has an average chemical composition very close to FeOOH with $M \sim 89$ g/mol. The mineral core has a mass density around $\sim 4.15 \pm 0.1$ g/cm^3, which is between that of feroxyhyte, goethite, and lepidocrocite. These results can be used to constrain structural models for Fh. Singly-coordinated surface groups dominate the surface of ferrihydrite ($\sim 6.0 \pm 0.5$ nm^{-2}). These groups can be present in two structural configurations. In pairs, the groups either form the edge of a single Fe-octahedron (~ 2.5 nm^{-2}) or are present at a single corner (~ 3.5 nm^{-2}) of two adjacent Fe octahedra. These configurations can form bidentate surface complexes by edge- and double-corner sharing, respectively, and may therefore respond differently to the binding of ions such as uranyl, carbonate, arsenite, phosphate, and others. The relatively low PZC of ferrihydrite can be rationalized based on the estimated proton affinity constant for singly-coordinated surface groups. Nanoparticles have an enhanced surface charge. The charging behavior of Fh nanoparticles can be described satisfactory using the capacitance of a spherical Stern layer condenser in combination with a diffuse double layer for flat plates.

1. INTRODUCTION

Ferrihydrite (Fh) is a natural nanoparticle. When freshly precipitated, the particles are extremely small, on the order of a few nm in diameter (Janney et al., 2000). Its reactive surface area is correspondingly high (Davis and Leckie, 1978). For this reason, small amounts of these nanoparticles may dominate the ion-binding properties of natural materials. Ion binding by ferrihydrite has been studied extensively (Dzombak and Morel, 1990). The mineral is considered as a proxy for the natural reactive oxide fraction of soils and sediments. Modeling the adsorption behavior of Fh is very challenging since the surface structure, as well as its composition, is largely unknown. It is difficult to determine the mineral structure of ferrihydrite unequivocally (Navrotsky et al., 2008). A standard model for the structure of ferrihydrite has been formulated (Drits et al., 1993), but a new crystal structure for ferrihydrite has recently been proposed (Michel et al., 2007). This structure

* Corresponding author. Fax: +31 317 41 9000.
E-mail addresses: tjisse.hiemstra@wur.nl (T. Hiemstra), willem.vanriemsdijk@wur.nl (W.H. Van Riemsdijk).

0016-7037/$ - see front matter © 2009 Elsevier Ltd. All rights reserved.
doi:10.1016/j.gca.2009.04.032

has been disputed by Rancourt and Meunier (2008) and Manceau (2009). Most studies do not focus on the surface structure and composition of ferrihydrite. The surface structure is important because ions can form various types of surface complexes by interacting with different types of surface sites.

For adsorbed ions, in-situ spectroscopy has identified different types of surface complexes and different combinations of surface sites are involved. For instance at the surface of goethite, Cd(II) ions may react with singly-coordinated surface groups forming double-corner complexes, but these ions may also form an edge-sharing complex by interaction with a combination of singly- and doubly-coordinated surface groups (Spadini et al., 1994, 2003). These two types of binding sites have a different affinity for the metal ion (Venema et al., 1996b). For ferrihydrite, ion binding at distinctly different types of sites can also be expected (Hiemstra et al., 2009). For instance, uranyl binds preferentially at the edges of Fe octahedra of ferrihydrite as a bidentate complex (Manceau et al., 1992) while ions such as carbonate, phosphate, and others may form double-corner bidentate complexes (Arai and Sparks, 2001; Hiemstra et al., 2004; Bargar et al., 2005). If the challenge is to link microscopic information to macroscopic adsorption data in a surface complexation model (SCM), then these differences in types of reactive sites must be defined, i.e. a multisite complexation (MUSIC) approach is needed.

A MUSIC model requires information about the proton affinity of the various types of surface groups. A complicating factor is that generally these affinities cannot be derived from classical acid–base titrations since the reactivity of the individual types of surface groups is totally overshadowed and suppressed by the action of the electrostatic field (Hiemstra et al., 1989). Therefore, theoretical or empirical models are necessary to estimate the intrinsic affinity and to provide constraints when describing experimental data. It has been suggested that the proton affinity is related to the degree of saturation of the oxygen charge by coordinating metals ions and protons, and an empirical model has been proposed to calculate the saturation. For calibration, a set of selected species in solution has been used and the model has successfully predicted the point of zero charge (PZC) of metal oxides (Hiemstra et al., 1996; Machesky et al., 2001). Ideally, the proton affinity constants can be obtained from "*ab-initio*" calculations for systems that are close to being realistic. A series of attempts has been made to apply a variety of theoretical approaches to this task (Rustad et al., 1996; Felmy and Rustad, 1998; Aquino et al., 2008) using the MUSIC model to describe the PZC and primary charge of iron oxide particles.

Nanoparticles may vary in size greatly. In some cases, the smallest particles can be considered as aqueous metal (hydr)oxide clusters with a well-defined number of metal ions and a well-known structure (Spiccia and Casey, 2007). A typical geochemical example is the Al_{13} hydroxide ion (Evans et al., 2008). In other cases, nanoparticles have been considered as nanocrystals with a rather well-defined mineral core and an additional surface region (Navrotsky, 2007). This surface region can change macroscopic properties such as the thermodynamic stability of the mineral (Navrotsky et al., 2008), and this is measurable even if the nanoparticles are still relatively large (~5–10 nm) and the surface areas relatively small (~100–200 m^2/g).

Freshly-prepared ferrihydrite is a rather exceptional nano oxide particle in the sense that the particles do not have a well-defined structure, and moreover, the particles are extremely small, i.e. 1.5–3 nm (Murphy et al., 1976; Janney et al., 2000). A considerable fraction of the metal ions is directly exposed at the surface (Manceau and Gates, 1997; Poulson et al., 2005) where they form the reactive surface sites. These surface sites are partly created by the chemisorption of water to complete the coordination sphere of the metal ions in the surface. For small particles, this site formation should be observable in macroscopic properties such as the molar mass and mass density. This will be analyzed theoretically in the present paper. We will show that the relationship between surface site densities and these macroscopic properties can be used to elucidate the chemical composition and mass density of the mineral core of a nanoparticle and may constrain the site densities of surface groups and *vice versa*.

The objective of this set of papers is to develop a suite of consistent relations between the microscopic and macroscopic descriptions of ferrihydrite, its surface structure, reactive site densities, primary charge, and its ion adsorption behavior. A quantitative MUSIC model will be developed in part I. In part II (Hiemstra et al., 2009), this model will be linked to the adsorption and interaction of ions that are supposed to react with different sets of surface sites. The latter approach can be very promising to understand the surface chemistry of Fh in general and it is a challenge to contribute to the elucidation of the surface structure with the help of SCM modeling if possible.

2. MUSIC: SURFACE STRUCTURE AND COMPOSITION

2.1. Surface structure

Freshly prepared iron oxide is almost X-ray amorphous and known as 2-line ferrihydrite. Relatively high temperatures, aging, dehydration, and (freeze-)drying may produce a more-structured 6-line ferrihydrite (Jambor and Dutrizac, 1998). The latter material can also be synthesized using ferritin protein cages (Kim et al., 2008). The structure of ferrihydrite has been described with different models, such as the standard model developed by Drits et al. (1993), and a new model recently proposed by Michel et al. (2007). An essential difference between both models is the multiphase character of the first model and the presence of tetrahedral Fe in the latter.

The fundamental unit of the recently proposed structure (Michel et al., 2007) is the δ-Keggin moiety with a tetrahedral coordinated Fe(III) in the center. Each oxygen ion of the tetrahedron is linked to three edge-shared Fe octahedra. This unit has only singly- and doubly-coordinated oxygens at the outside. In its idealized form, this Fh structure is isostructural with akdalaite (Michel et al., 2007) and its synthetic counterpart tohdite (Yamaguchi et al., 1964). These minerals ($5Al_2O_3{\cdot}H_2O$) may have a (sub)euhedral morphol-

ogy with a basal 00(0)1 plane (Yamaguchi et al., 1964) that is bounded by the 1 −1 (0) 0 face and the 1 −1 (0) 1 face (Hwang et al., 2006) and its equivalents.

At the isostructural 0 0 1 face of the recently proposed Fh structure (Michel et al., 2007), only doubly-coordinated surface groups (13 nm^{-2}) are found if the crystal is terminated without breaking the Keggin moiety (no tetrahedral Fe at the surface). The isostructural 1 −1 0 face of Fh has singly-, doubly-, and triply-coordinated surface groups. Equal numbers of singly- and doubly-coordinated surface groups (5.6 nm^{-2} each) are present. If the Keggin unit is maintained at this crystal termination, the density of the triply-coordinated surfaces groups is 7.5 nm^{-2}. The isostructural 1 −1 1 face has the same composition.

In the standard model, ferrihydrite is a multiphase material. According to this model, the local structure of freshly-prepared ferrihydrite (Fh) may partly resemble that of goethite (Drits et al., 1993; Spadini et al., 1994). Similarly as with goethite, two characteristic Fe–O bond lengths are found (Combes et al., 1989; Waychunas et al., 1993; Rose et al., 1997; Ulrich et al., 2006), i.e. $d_{FeO} \approx 195 \pm 1$ pm and $d_{FeOH} = 209 \pm 1$ pm. In this model, the fundamental unit of synthetic 2-line ferrihydrite is the $Fe(O,OH)_6$ octahedron. According to Drits et al. (1993), the octahedra are linked together in short single and double chains, which are cross-linked irregularly to form micro-domains. The oxygen arrangement in the standard model is based on hexagonal (ABA) and cubic (ABC) stacking as found in goethite and lepidocrocite, respectively. In the case of Fh, the main stacking is ABACA. In goethite (α-FeOOH) and lepidocrocite (γ-FeOOH), half of the octahedra is occupied with Fe but in Fh, the distribution is irregular (Manceau, 2009). In addition, a stacking as in feroxyhyte (δ-FeOOH) is assumed. Nano-diffraction supports the standard model (Janney et al., 2001).

In the standard model, goethite can be chosen as a proxy to understand the surface reactivity of ferrihydrite (Spadini et al., 1994, 2003). Goethite is needle- or lath-shaped and bounded by 1 1 0 and 1 0 0 faces (Weidler et al., 1999; Gaboriaud and Ehrhardt, 2003). The needles have predominantly 1 1 0/1 0 0 faces which consist of long chains of octahedra terminated at the top end by representative faces such as the 0 0 1 and 0 2 1 faces. However, in the case of nanoparticles, the chains of octahedra are very short and ferrihydrite particles are close to spherical, and not elongated or needle-like. For a particle with a typical diameter of ~1.5–3 nm, the maximum number of octahedra in a chain is only, respectively, ⩽~5–10. For spherical particles, the contribution of the 1 1 0/1 0 0-like patches is smaller and that of the 0 0 1/0 2 1-like patches larger than for needle-shaped particles. Note that the above indices for the various crystal faces of goethite refer to the Pbma space group (Manceau et al., 2000) as used in the Inorganic Crystal Structure Database (ICSD, 2008).

The 1 1 0 face of goethite contains rows of singly- (≡FeOH), doubly- ($\equiv Fe_2OH$), and triply-coordinated surface groups ($\equiv Fe_3O$) (Hiemstra et al., 1996). The variable charge is due to protonation and deprotonation of the singly- ($\equiv FeOH^{-1/2}$) and triply- ($\equiv Fe_3OH^{+1/2}$) coordinated surface groups, both of which have an effective site density of about 3 nm^{-2} (Hiemstra et al., 1996).

The structure and composition of two representative faces (0 0 1 and 0 2 1 face) that terminate the chains of octahedra of goethite are shown in Fig. 1. Both surfaces have equal numbers of singly- (≡FeOH) and doubly- ($\equiv Fe_2OH$) coordinated surface groups. The site densities on the faces are similar, i.e. 7.5 nm^{-2} (0 2 1 face) and 8.8 nm^{-2} (0 0 1 face) for each type of surface group. A major difference between these two faces is their structure. The 0 0 1 face consists of pairs of singly-coordinated surface groups that form the edges of a limited set of Fe octahedra while the 0 2 1 face consists of singly-coordinated surface groups present at the corners of adjacent octahedra (Fig. 1). A similar difference in surface structure is also found in lepidocrocite where the singly-coordinated surface groups form either edges or adjacent double corners at the 1 0 0 and 0 0 1 faces, respectively. The fundamental difference in surface structure with respect to the presence of singly-coordinated

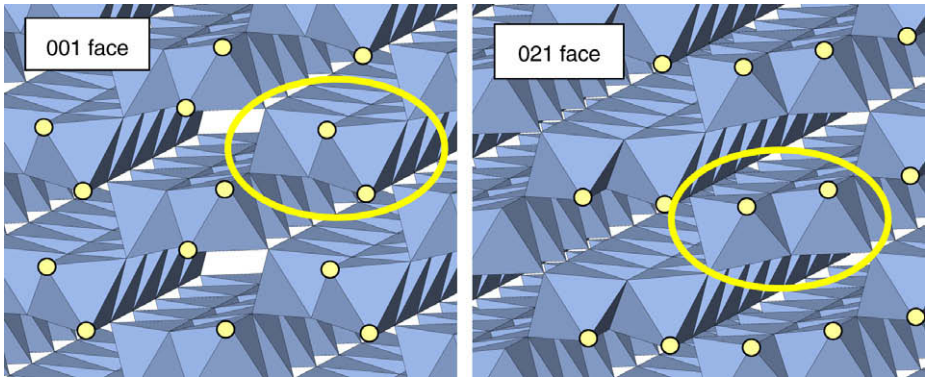

Fig. 1. The composition and octahedral structure of the 0 0 1 and 0 2 1 faces of goethite that have been used as a model for explaining the difference in reactivity of singly-coordinated surface groups (yellow spheres). For both faces, termination of the double chains of Fe octahedra results in the presence of singly- and doubly-coordinated surface groups in a 1:1 ratio. On the 0 0 1 face, the singly-coordinated surface groups are present in pairs on each octahedron, forming an edge, while when they are present on the 0 2 1 face, they are located on adjacent octahedra with single corners. Bidentate complexation via interaction with singly-coordinated surface groups is only possible by edge sharing on the 0 0 1 face and by double-corner complex formation on the 0 2 1 face. (For interpretation of the references to color in this figure legend, the reader is referred to the web version of this paper.)

surface groups in the form of edges or double corners can lead to a very different reactivity towards particular ions (Manceau et al., 2000; Hiemstra et al., 2009).

2.2. Structure and binding

Some oxyanions are able to form double-corner bidentate complexes by interacting with singly-coordinated surface groups present at the corners of two adjacent octahedra. A classical example is the binding of phosphate (Tejedor-Tejedor and Anderson, 1990; Arai et al., 2001). Carbonate may also form double-corner complexes (Hiemstra et al., 2004; Bargar et al., 2005). Other examples are arsenate (Waychunas et al., 1996; Farquhar et al., 2002; Sherman and Randall, 2003; Majzlan et al., 2007) and arsenite (Ona-Nguema et al., 2005) as has been observed with EXAFS for goethite and ferrihydrite. These complexes may form at both the 1 1 0/1 0 0 and the 0 2 1 faces of goethite. According to the above analysis, the double-corner complexes will not be formed at the 0 0 1 face of goethite (Fig. 1, left). Bidentate complex formation is possible at the 0 0 1 face but only via edge sharing. Edge sharing has been reported for arsenite (Ona-Nguema et al., 2005) and is also found for uranyl (Manceau et al., 1992; Waite et al., 1994; Ulrich et al., 2006; Rossberg et al., 2009).

We may also analyze this aspect of the reactivity of Fh using as proxy the recently proposed mineral structure of Michel et al. (2007). The idealized 0 0 1 face has only singly- and doubly-coordinated surface groups that in combination form the edges of the octahedrons. Both other faces, the 1 −1 0 and 1 −1 1 face, have a composition that allows formation of double-corner complexes because singly-coordinated surface groups are present in pairs at adjacent corners. However, all mentioned faces do not have edges with pairs of singly-coordinated surface groups that are able to form bidentate surface complexes by edge sharing with uranyl (Hiemstra et al., 2009). Large numbers of octahedral edges having two singly-coordinated surface groups can only be rationalized when additional Fe octahedra are linked to the crystal terminations or assuming many defects.

2.3. Site densities

The above discussion shows that singly-coordinated surface groups may react to form distinct types of complexes and for this reason, at least two types of ≡FeOH groups have to be distinguished in surface complexation modeling. Unfortunately, the number of singly-coordinated surface groups that should be attributed to each category is unknown, particularly for ferrihydrite where information about the precise structure of the nanoclusters, their representative crystal faces and patches, as well as their composition is lacking. Nevertheless, some estimates will be made to constrain possible numbers derived in other ways. Based on the above analysis and later results, we give credit to the standard model as proxy.

Ferrihydrite particles apparently have an almost spherical shape. The particles may have some anisotropic properties in the sense that on aging there is a tendency of the particles to orientate in rows (Murphy et al., 1976; Burleson and Penn, 2006). If the shape of a spherical particle is constructed from 1 1 0- and 0 2 1-like faces, then approximately equal contributions of both types of faces will be found. In addition, 0 0 1-like terminations will be present. In the case of an equal contribution of both types of terminating (0 2 1 and 0 0 1) faces, the total number of singly-coordinated surface groups on the 1 1 0 + 0 2 1 + 0 0 1 faces will be $0.5 * 3\ nm^{-2} + 0.25 * 7.5\ nm^{-2} + 0.25 * 8.8\ nm^{-2} = 1.5 + 1.9 + 2.2 = 5.6\ nm^{-2}$. Irregularities and defects in the actual structure may reduce the contribution of sites with a high metal coordination as found on the 1 1 0 faces. Moreover, at a decrease to a very small particle size, the number of sites that are common at two or more crystal faces will increase and these common sites have a lower metal coordination too. Therefore, the fraction of sites representative for the 1 1 0/1 0 0 faces may decrease (<0.5) and the fractions representative for the 0 2 1 and 0 0 1 faces may increase (>0.25). If this is equivalent with for instance an equal contribution of patches representative for the three mentioned faces, the site density on the 1 1 0 + 0 2 1 + 0 0 1 faces will be $0.33 * 3\ nm^{-2} + 0.33 * 7.5\ nm^{-2} + 0.33 * 8.8\ nm^{-2} = 1.0 + 2.5 + 2.9 = 6.4\ nm^{-2}$. Based on these calculations, the site densities (N_s) of ≡FeOH that may form double-corner (c) and edge (e) complexes are estimated for the standard model. The former value is found by summation of the average values of the calculated site densities at the 1 1 0 and 0 2 1 faces for the two choices of the above face distributions, leading to $N_s(c) = 3.5 \pm 0.1$ and the latter value is the average value for the 0 0 1 face, i.e. $N_s(e) = 2.5 \pm 0.4\ nm^{-2}$. According to our sensitivity analysis, the greatest variation is for the sites that may bind ions as an edge-sharing complex.

At each of the above crystal faces, the singly- and doubly-coordinated surface groups are present in a 1:1 ratio. Therefore, the total site density of the doubly-coordinated surface groups (≡Fe_2OH) is equal to the sum of the singly-coordinated surface groups i.e. N_s (≡Fe_2OH) = $6.0 \pm 0.5\ nm^{-2}$. These doubly-coordinated surface groups are assumed to have no significant proton reactivity in the pH range around neutral (Hiemstra et al., 1996).

The total site density for the ≡FeOH and ≡Fe_2OH sites at the 1 1 0/1 0 0 faces of goethite is much smaller than for the 0 2 1/0 0 1 faces, and this is related to the presence of a considerable number of triply-coordinated groups ≡Fe_3O(H) at the 1 1 0/1 0 0 faces. Actually, two types of triply-coordinated groups exist. Both types of groups differ strongly in proton affinity as follows from the MUSIC model but this can also be understood directly from the structure of FeOOH. The oxygens in goethite are all triply-coordinated, but one of them accepts a proton (OH) and the other not (O). Both types of oxygens are also found at the 1 1 0 face. The total site density of the triply-coordinated surface groups at the 1 1 0/1 0 0 face is $9\ nm^{-2}$. However, it can be shown that effectively the proton reactivity is less due to the large difference in proton affinity of both types of triply-coordinated surface groups (Hiemstra et al., 1996). Therefore, the effective site density is only $3\ nm^{-2}$. Using the above face/patch distribution, the

overall effective site density of $\equiv Fe_3O(H)$ can be estimated as $N_s(tr) = 1.2 \pm 0.2\ nm^{-2}$. The total site density of all proton reactive groups, N_s ($\equiv FeOH + \equiv Fe_3O$), is therefore $7.2 \pm 0.7\ nm^{-2}$ in the case of goethite as proxy for the standard model.

It is important to note that the reactive site density is difficult to estimate experimentally from a saturation of the surface sites with ions. Attempts to determine the site density of singly-coordinated surface groups of goethite with the fluoride ion showed that at high concentrations doubly-coordinated surface groups might also be involved (Hiemstra and Van Riemsdijk, 2000). The use of protons to derive the site density of the proton reactive surface groups is also questionable. Even in the case of an extremely large pH window, it is not possible to reach site saturation as recently shown for goethite (Lutzenkirchen et al., 2002). The reason for this difficulty is the strong suppression of proton adsorption by the surrounding electrostatic field, itself created by proton adsorption. With the generalized two-layer (GTL) model for Fh (Dzombak and Morel, 1990), a site density has been derived by fitting. In the GTL model, the so-called Stern layer is absent and this will lead in the model to an exceptionally high proton loading at low pH, which is not shown by the data. The absence of a Stern layer in the model has to be compensated by using a low site density that limits the proton loading (Venema et al., 1996a). Therefore, this low site density can be considered as an artifact brought about by the limitations of that model.

2.4. Proton adsorption

In modeling, the charge on individual crystal faces may be treated separately (Ponthieu et al., 2006), but in the present approach, ferrihydrite is treated electrostatically as a single surface. This assumes that individual patches all experience the same smeared-out potential. A rationale for this is that the extent of the double layer (several nm) can be quite large in relation to the size of the Fh nanoparticles and the distribution of the patches. This leads to a large degree of double layer overlap between the individual patches.

As with goethite, the protonation reactions for ferrihydrite are described by:

$$\equiv FeOH^{-1/2} + H^+(aq) \Longleftrightarrow \equiv FeOH_2^{+1/2} \quad (1)$$

$$\equiv Fe_3O^{-1/2} + H^+(aq) \Longleftrightarrow \equiv Fe_3OH^{+1/2} \quad (2)$$

Doubly-coordinated surface groups are probably not proton reactive in the usual experimental pH window. This assumption is strongly supported by experimental evidence. On freshly-cleaved 0 0 (0) 1 faces of hematite, no charge is developed over a large pH range (Eggleston and Hochella, 1992; Hiemstra and Van Riemsdijk, 1999), in contrast to other crystal faces of hematite that generally will charge. This strong anisotropic spread of charge is supported by recent cryogenic-XPS measurements (Shchukarev et al., 2007). In addition, an extremely low reactivity for phosphate (Colombo et al., 1994) is found in those preparations of synthetic hematite that have a large contribution of basal planes (0 0 1 face). This is also found for sulfate (Sugimoto and Wang, 1998; Hiemstra and Van Riemsdijk, 1999). However, we also note that synthetic single-crystals of Fe_2O_3 with an exposed 0 0 (0) 1 face may certainly show reactivity. In these cases, the reactivity is due to the presence of singly-coordinated surface groups rather than doubly-coordinated surface groups, for instance as result of the presence of adatoms or a different crystal termination (Waychunas et al., 2006).

According to the MUSIC model (Hiemstra et al., 1996; Venema et al., 1998), the proton affinity ($\log K_H$) of the singly- (Eq. (1)) and the reactive triply- (Eq. (2)) coordinated groups may be close to $\log K_H \sim 8$ and $\log K_H \sim 11.7$, respectively, for goethite. This suggests that the singly-coordinated groups are the more acidic. The relative abundance of both types of surface groups, expressed as the fraction $f_{FeOH} = N_s(FeOH)/N_s(FeOH + Fe_3O)$, will determine the point of zero charge (PZC), provided that the doubly-coordinated groups, $\equiv Fe_2OH^0$, remain uncharged.

Mathematically, the corresponding relationship is (Venema et al., 1998):

$$f_{FeOH} = \left\{ \frac{(H^+)_{PZC} K_{Fe_3O}}{1 + (H^+)_{PZC} K_{Fe_3O}} - \frac{1}{2} \right\} \Bigg/ \left\{ \frac{(H^+)_{PZC} K_{Fe_3O}}{1 + (H^+)_{PZC} K_{Fe_3O}} - \frac{(H^+)_{PZC} K_{FeOH}}{1 + (H^+)_{PZC} K_{FeOH}} \right\} \quad (3)$$

in which $(H^+)_{PZC}$ is the aqueous proton activity at the PZC. The relationship between the relative abundance of surface groups and the PZC is given in Fig. 2 as a line. This can be compared with the data.

For goethite as a whole, the fraction of singly-coordinated surface groups is slightly greater than 0.5. The

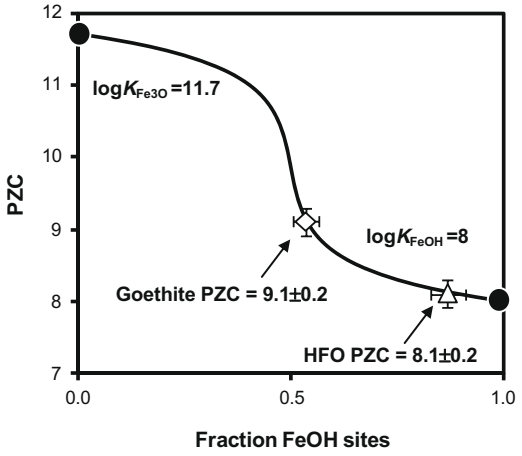

Fig. 2. The PZC as a function of the relative abundance of singly-coordinated ≡FeOH surface groups calculated (Eq. (3)) assuming proton affinity constants for singly- and triply-coordinated surface groups as estimated with the MUSIC model (Venema et al., 1998). Open symbols show the estimated fraction of FeOH and experimental PZC of goethite of 9.1 (diamond) and 2-line Fh (PZC = 8.1, triangle). The black spheres represent the calculated PZC for a surface with only one type of reactive site having a $\log K_H$ as indicated.

presence of ~5% top-end faces (0 2 1 + 0 0 1) leads to a PZC value of about 9.1 ± 0.2 which is below the average log K_H value (~9.8) for a 1:1 ratio. Increasing the abundance of singly-coordinated groups will decrease the PZC until it approaches about PZC ~ 8. This is consistent with the experimentally-observed PZC values (~8.1 ± 0.2) of freshly-prepared ferrihydrites (Davis and Leckie, 1978; Hsi and Langmuir, 1985; Dzombak and Morel, 1990). For ferrihydrite, aged for 3 weeks, a higher value of the PZC has been reported. Based on the reported proton *concentration* (ph = 8.2) at zero charge, the PZC is ~8.25 (Spadini et al., 2003). This slightly higher PZC of aged Fh might be due to a smaller fraction of singly-coordinated surface groups.

As mentioned above, a number of attempts has been made applying theoretical methods to predict the proton affinity constants of surface groups (Rustad et al., 1996; Felmy and Rustad, 1998; Rustad and Felmy, 2005; Aquino et al., 2008). In a recent approach (Aquino et al., 2008), the protonation of aqueous Fe monomers as well as surface species was calculated with an ab-initio molecular orbital approach which explicitly included hydration. The affinity of the various monomeric Fe-hydroxyl species in solution was predicted and compared to experimental data. This showed a deviation of only $\Delta \log K_H \leqslant \sim 1$–3 units, which is promising.

In general, such a test is more problematic for surface groups because the protonation of the surface is the result of the interplay of various types of surface groups and is strongly masked by the electrostatic field. Usually, the predicted value of the PZC is used as a first test. In the particular case of TiO_2, FTIR data have also been used, and these showed good agreement with predictions from the MUSIC model (Hiemstra and Van Riemsdijk, 2002). For the 1 1 0 face of goethite, the estimated PZC is 9.8 when calculated from the predicted log K_H values of Aquino et al. (2008) using a full speciation model (Hiemstra et al., 1996) with equal site densities for the singly-, doubly-, and triply-coordinated surface groups. This predicted PZC is the same as the value predicted from the MUSIC model, but the individual log K_H constants are rather different. In particular, the newly-predicted log K_H for ≡FeOH is relatively high (log K_H = 12.1) compared to the value used in Fig. 2 (log $K_H \sim 8$). With the lower log K_H value predicted by the MUSIC model, the lower PZC values of Fh and goethite can be understood within a single framework (Fig. 2). Fh samples are probably dominated by singly-coordinated surface groups and the low PZC of Fh suggests that these surface groups are rather acidic. However, note that the presently derived structural MUSIC model of Fh is a simplification at the molecular level and definite conclusions cannot be drawn yet.

Although singly- and triply-coordinated groups may differ in their proton affinity, the description of the charging behavior of e.g. goethite can be simplified by assuming log K_H = PZC (Hiemstra et al., 1996). This approach can also be used for ferrihydrite (Table 1) and will be applied below after introducing the double layer model.

2.5. Double layer model

The adsorption of ions at charged surfaces is usually strongly affected by electrostatic interactions. The location of the ionic charge in the electrostatic double layer (EDL) is very important for calculating the energy involved in these electrostatic interactions. The EDL used in this study consists of two Stern layers (Fig. 3). A series of measurements (Pashley and Israelachvili, 1984; Fenter and Sturchio, 2004; Catalano et al., 2006) and calculations (Predota et al., 2004; Koppen and Langel, 2006) have shown that the water molecules near a flat mineral surface are usually ordered in several layers. Currently, we assume that water structuring will also be present around Fh nanoparticles. Near a charged surface, electrolyte ions can only move in discrete steps towards the minimum distance of approach (Pashley and Israelachvili, 1984). In contrast, several water layers away from the surface, the electrolyte ions are present in a diffuse pattern known as the diffuse double layer (DDL). This molecular picture can be linked to macroscopic observations. As described by Hiemstra

Table 1
Tableau defining the surface components of the primary charging reactions. The proton charge is attributed to the surface (Δz_0), the electrolyte ion charge to the 1-plane (Δz_1), no charge is added to the 2-plane ($\Delta z_2 = 0$) (Extended Stern layer model with $C_1 = 1.15$ F/m^2, $C_2 = 0.9$ F/m^2).

Species[a]	≡FeOH$^{-1/2}$ [b]	≡Fe$_3$O$^{-1/2}$ [b]	Δz_0	Δz_1	Δz_2	log K[c]
≡FeOH$_2^{+1/2}$	1	0	1	0	0	log K_H = +8.06
≡FeOH$^{-1/2}$–Na$^+$	1	0	0	1	0	log K_{Na} = −0.60
≡FeOH$_2^{+1/2}$–Cl$^-$	1	0	1	−1	0	log K_H + log K_{Cl} = +7.61
≡FeOH$_2^{+1/2}$–NO$_3^-$	1	0	1	−1	0	log K_H + log K_{NO_3} = +7.38
≡FeOH$_2^{+1/2}$–ClO$_4^-$	1	0	1	−1	0	log K_H + log K_{ClO_4} = +6.36
≡Fe$_3$OH$^{+1/2}$	0	1	1	0	0	log K_H = +8.06
≡Fe$_3$O$^{-1/2}$–Na$^+$	0	1	0	1	0	log K_{Na} = −0.60
≡Fe$_3$OH$^{+1/2}$–Cl$^-$	0	1	1	−1	0	log K_H + log K_{Cl} = +7.61
≡Fe$_3$OH$^{+1/2}$–NO$_3^-$	0	1	1	−1	0	log K_H + log K_{NO_3} = +7.38
≡Fe$_3$OH$^{+1/2}$–ClO$_4^-$	0	1	1	−1	0	log K_H + log K_{ClO_4} = +6.36

[a] Doubly-coordinated sites (≡Fe$_2$OH^0) have been omitted since they do not contribute to the surface charge. See Section 2.4.
[b] Singly-coordinated groups are present as ≡FeOH(e) (N_s(e) = 2.5 nm^{-2}) as well as ≡FeOH(c) (N_s(c) = 3.5 nm^{-2}), i.e. $\Sigma\ N_s(\text{FeOH}^{-1/2}) = 6.0$ nm^{-2}, see text. The effective site density of Fe$_3$O$^{-1/2}$ is N_s(tr) = 1.2 nm^{-2}.
[c] The ion pair formation constants are from Hiemstra and van Riemsdijk (2006). The log K_H was fitted (Fig. 4).

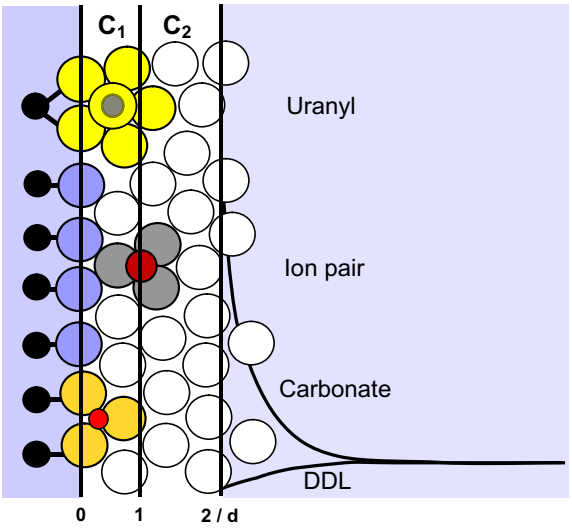

Fig. 3. Schematic diagram of the double layer structure of the Extended Stern layer model showing a metal (hydr)oxide surface (black spheres coordinating with surface oxygens) and the position of bidentate inner sphere complexes of uranyl and carbonate that both distribute their charge between the 0- and 1-planes (vertical lines) of the inner Stern layer. The outer sphere complexes of electrolyte ions such as NO_3^- and Na^+ (ion pairs) locate their charge in the 1-plane (vertical line in the middle). The DDL is separated from the 1-plane by an outer Stern layer with a capacitance C_2 ($C_2 \sim 0.9 \pm 0.2$ F/m^2). The curved lines illustrate the non-scaled concentrations of counter- and co-ions in the DDL, starting at the 2- or *d*-plane. Inner sphere complexes like carbonate or uranyl distribute their charge between the 0- and 1-plane, see part II (Hiemstra et al., 2009).

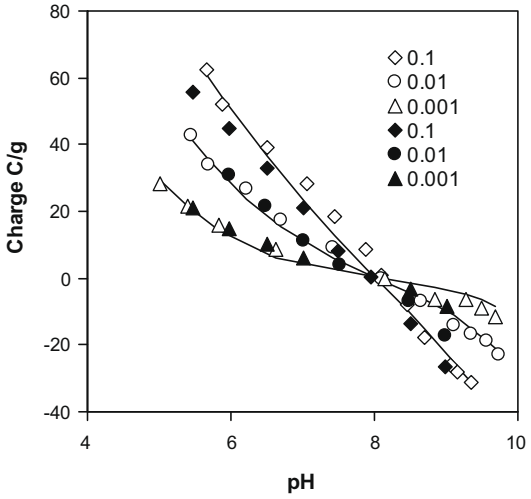

Fig. 4. The surface charge of ferrihydrite at three electrolyte concentrations measured by Davis (1977) (closed symbols) as given in Dzombak and Morel (1990) and by Hsi and Langmuir (1985) (open symbols). The lines have been calculated using a total site density for protons of 7.2 nm^{-2}. The Stern layer capacitances are $C_1 = 1.15$ F/m^2 (spherical condenser, Eq. (4)) and $C_2 = 0.9$ F/m^2 (Fig. 3) The ion pair formation constants are from Table 1 and log K_H (=8.06) has been fitted. The calculated lines are valid for a reactive surface area of $A = 650$ m^2/g.

and Van Riemsdijk (2006), the interpretation of a consistent set of proton titrations of goethite suspensions, performed in range of electrolytes, showed that the data could only be explained well by assuming that the DDL is separated from the minimum distance of approach by a Stern layer with a capacitance of $C_2 = 0.9 \pm 0.2$ F/m^2. This EDL model can be called an Extended Stern (ES) model (Fig. 3). This interpretation also rationalizes the revised TL model used by Sverjensky (2005).

2.6. Primary charge and surface area

The charging behavior of freshly-prepared ferrihydrite (aged 4 h) has been studied by Davis and Leckie (1978) and Hsi and Langmuir (1985). The results are given in Fig. 4. The Fh has been produced in both cases using NaOH free of carbonate, but explicit exclusion of CO_2 during the titration has not been reported. Transmission Electron Microscopy (TEM) suggests the presence of individual nanoparticles in freshly prepared Fh. However, it aggregates upon aging (Murphy et al., 1976; Burleson and Penn, 2006) resulting in alignment of particles and a gradual fusion after a number of days. Such a process will reduce the number of available sites per mass unit and correspondingly the surface charge (C/g). One of the problems of nanoparticles is the uncertainty in their reactive surface area. Typical values of the BET surface area for Fh are 200–350 m^2/g (Dzombak and Morel, 1990). However, the validity of the N_2 gas adsorption approach may be questioned because of the strong effect of drying which could result in a large area of contact between particles and a lower surface area than in the original suspension. Therefore, Davis and Leckie (1978) suggested using the charging behavior of ferrihydrite as a measure of the surface area (m^2/g) by comparing the calculated surface charge (C/m^2) to the experimental one (C/g). Following this approach, the surface charge has been calculated using the ion pair formation constants (Table 1) reported for goethite and a specifically chosen inner Stern layer capacitance of $C_1 = 1.15$ F/m^2, which represents the Stern layer properties of nanoparticles, as discussed in detail below (Section 2.6.2). The outer Stern layer capacitance has been set at $C_2 = 0.9$ F/m^2 (Fig. 3) and the total site density of the proton reactive surface groups set at $N_s = 7.2$ nm^{-2} (Section 2.3). The calculated results are given in Fig. 4 as lines.

2.6.1. Surface area

The observed and calculated values agree in the case of a specific surface area of $A = 650$ m^2/g and so this value has been used in our subsequent data analysis and in the modeling of ion adsorption by freshly prepared 2-line Fh as described in part II (Hiemstra et al., 2009) unless stated differently. We note that aging as well as Fh preparation at a relatively high initial Fe concentration may result in a smaller surface area (Davis and Leckie, 1978). Ferrihydrite, aged 24 h and produced at a relatively high Fe concentration (Girvin et al., 1991), had a lower surface area (450 m^2/g) when calculated with the above approach. Of

course, these estimated surface areas will also depend on the assumed capacitance of the Stern layer. The actual value is unknown. For instance, surface roughness (Hiemstra et al., 1989; Van Hiemstra and Riemsdijk, 1991; Boily et al., 2001) may result in a greater charge and a correspondingly larger capacitance when modeled. In the case of a capacitance of $C_1 = 1.5$ F/m^2, the estimated surface area of freshly prepared Fh would be ~550 m^2/g instead of ~650 m^2/g. The estimated surface areas by fitting are consistent wit the particle size (Section 2.7).

2.6.2. Spherical double layer

In the above analysis, for practical reasons, the calculations were done using a flat double layer structure. However, the analysis also shows that the surface area is very large which suggests that the freshly prepared 2-line Fh consists of tiny nanoparticles (Section 2.7). For such small particles, the double layer is relatively curved. One may argue that for this reason the use of a spherical double layer model (Stern layer and DDL) is more appropriate. The effect of a spherical double layer on the charging behavior has recently been evaluated (Abbas et al., 2008) using Monte Carlo simulations. A clear effect of particle size was predicted. In our own (SCM) calculations with spherical double layer theory, we have included ion pair formation. Indeed, the surface charge is higher. However, our modeling also shows that the use of a spherical DDL layer is often ($I \geqslant \sim 10^{-2}$ M) not essential for the description of charging behavior. The reason is that most of the surface charge is neutralized in the compact part of the double layer due to the presence of ion pairs. The higher surface charge of nanoparticles (~10%) is mainly due to the presence of a curved Stern layer. The capacitance of a spherical condenser C_r of a particle with radius r and thickness Δr of the Stern layer is related to the capacitance C of a flat plate according to:

$$C_r = \frac{r + \Delta r}{r} C \tag{4}$$

Two-line Fh may have an average particle size of ~2.6 nm, i.e. $r \sim 1.3$ nm (Section 2.7). In combination with a Stern layer thickness of $\Delta r = 0.35 \pm 0.05$ nm and a capacitance of 0.9 F/m^2 for a flat plate (Hiemstra and Van Riemsdijk, 2006), the equivalent capacitance value for the spherical condenser is $C_r \sim 1.15$ F/m^2. In the case of 6-line Fh ($r \sim 3$ nm), the value will be 1.0 F/m^2.

In the above calculations, one assumes the same dielectric properties. It can be shown that the capacitance C_r of a spherical double layer is proportional with the relative (ε_r) and absolute (ε_o) dielectric constant according to:

$$C_r = \varepsilon_r \varepsilon_o \frac{r + \Delta r}{r \Delta r} \tag{5}$$

The linear relationship implies that small differences in the relative dielectric constant ε_r have a relatively large effect on the capacitance C_r. To our knowledge, any influence of curvature on the dielectric properties is unknown. In the final calculations (Fig. 4), we applied the standard double layer theory (flat plate) but used an enhanced Stern layer capacitance of $C = 1.15$ F/m^2 (Eq. (4)), which results in a satisfying and practical description of the main electrostatic double layer properties of the nanoparticles.

2.7. Particle size

As mentioned in the Introduction, ferrihydrite can be considered as a rather exceptional nano oxide particle in the sense that the particles can be extremely small and therefore will have a large surface area. For non-porous spherical particles, the particle diameter d (m) and specific surface area A (m^2/g) are related according to:

$$d = \frac{6}{\rho A} \tag{6}$$

in which ρ is the mass density (g/m^3). A specific surface area of 650 m^2/g is equivalent to a spherical particle diameter of $d \sim 2.6 \pm 0.1$ nm in the case of a mass density ρ of 3.5 ± 0.1 g/cm^3 as reported for 2-line ferrihydrite (Murphy et al., 1975, 1976). This calculated size falls in the range of values ($d = 1.5$–3 nm) measured for the diameter of apparently spherical particles (Murphy et al., 1976; Janney et al., 2000). The typical size of 6-line ferrihydrite particles is significantly larger, i.e. $d = 5$–6 nm (Janney et al., 2000). At a mass density ρ of 3.96 cm^3/g (Towe and Bradley, 1967), this is equivalent to a surface area of $A = 330$–270 m^2/g, provided that the particles are non-porous.

The above particle sizes can be used for calculating the number of Fe atoms present in the various particles, i.e. using $1/6\pi d^3 \rho N_{av}/M$ in which N_{av} is Avogadro's number and M the molar mass (Section 2.8). For 2L-Fh ($d = 2.6$ nm), this gives an average of only ~200 Fe/particle while for 6L-Fh the number is much higher, i.e. ~1600 ($d = 5$ nm), ~2800 ($d = 6$ nm), and ~4500 Fe/particle ($d = 7$ nm). These numbers approximately agree with experimental data (Kim et al., 2008).

2.8. Molar mass

The molar mass M of goethite, lepidocrocite, and feroxyhyte (respectively, α-, γ-, δ-FeOOH) is 89 g/mol Fe. For nanoparticles with essentially the same structure but a larger surface area, a greater molar mass per Fe is expected since surface groups will make up a significant contribution. Part of the structure of surface groups of nanoparticles is formed by the chemisorption of water completing the coordination sphere of Fe at the surface. In the hypothetical extreme of a size reduction to a single octahedron, i.e. $Fe(OH)_3(OH_2)_3$, the molar mass would increase to 161 g/mol Fe.

In the case of the formation of two imaginary surfaces by cleaving a Fe–O bond network, the oxygens would be distributed over both surfaces. The reduced coordination of the metal ions can be restored by the uptake of H_2O. The number of water molecules involved, N_{H_2O} (nm^{-2}), depends on the change of the coordination number (ΔCN) of the various surface groups created in comparison to the coordination number of the oxygen before cleavage (CN). The overall number of water molecules (N_{H_2O}) can be calculated with:

$$N_{H_2O} = \sum_j \frac{\Delta CN_j}{CN} N_{s,j} \quad (7)$$

in which $N_{s,j}$ is the site density (nm^{-2}) of the various surface groups of type j, i.e. N_{H_2O} is surface composition dependent. For a mineral like goethite, the formation of the 1 1 0 face leads to $N_{H_2O} = 3\ nm^{-2}$ (Eq. (7)), and for the 0 2 1 and 0 0 1 faces, these are $N_{H_2O} = 7.5\ nm^{-2}$ and $N_{H_2O} = 8.8\ nm^{-2}$, respectively. For 2-line ferrihydrite, the amount of additionally coordinated water can be calculated based on the above-estimated surface composition, resulting in $N_{H_2O} = 6.0 \pm 0.5\ nm^{-2}$. Experimentally, such a value is typically found for oxides in general (Navrotsky et al., 2008).

In the case of a surface area of $A = 650\ m^2/g$ Fh, the amount of chemisorbed water ($N_{H_2O} = 6.0 \pm 0.5\ nm^{-2}$) is equal to 0.12 ± 0.01 g H_2O/g Fh. Per gram, ferrihydrite will contain 0.12 g chemisorbed H_2O and 0.88 g mineral core (e.g. FeOOH). The latter is equivalent to 9.9 mmol Fe per gram Fh and this yields a molar mass for the nanoparticles of $M \sim 101 \pm 1$ g/mol Fe. In general, the molar mass of nanoparticles M_{nano} is:

$$M_{nano} = \frac{M_{core}}{\left(1 - \frac{N_{H_2O} A}{N_{av}} M_{H_2O}\right)} \quad (8)$$

in which M_{core} is the molar mass of the mineral core of the nanoparticles (g/mol), M_{H_2O} the molar mass of water (18 g/mol), N_{H_2O} the site density of additional water (Eq. (7)) to complete the metal ion coordination at the surface (m^{-2}), and N_{av} is Avogadro's number (mol^{-1}).

The molar mass as a function of the specific surface area of the nanoparticles (Eq. (8)) has been given as a line in Fig. 5 using $M_{core} = 89$ g/mol and assuming a constant surface site density. For a large particle size and a corresponding low surface area (Eq. (6)), the molar mass of the nanoparticles (M_{nano}) will approach the molar mass for the mineral core M_{core}, A strongly enhanced molar mass ($M_{nano} = 101 \pm 1$ g/mol Fe) is calculated for small ferrihydrite particles with a surface area of $A = 650\ m^2/g$ (Fig. 5). Larger Fh particles with a lower surface area of for instance about a half ($A \sim 350\ m^2/g$) or one-third ($A \sim 233\ m^2/g$) have calculated molar masses of $M_{nano} \sim 95$ or ~93 g/mol Fe, respectively. These lower values are close to the molecular mass given by the classical chemical compositions suggested for Fh, e.g. $5Fe_2O_3{\cdot}9H_2O$, $Fe_5(O_4H_3)_3$, or $Fe_2O_3{\cdot}2FeOOH{-}2.6H_2O$ (Schwertmann and Taylor, 1989) that all can be reduced to approximately $FeOOH{-}0.4H_2O$ with $M_{nano} = 96$ g/mol Fe. The experimental upper and lower limits of the molar mass of Fh can also be estimated from recent data (Mikutta et al., 2008; Rancourt and Meunier, 2008) resulting in $M_{nano} \sim 102 \pm 2$ g/mol Fe for 2-line ferrihydrite (2L-Fh) and $M_{nano} \sim 92$ g/mol Fe for 6-line ferrihydrite (6L-Fh).

The average of the above data is given as open squares in Fig. 5 where they are plotted against the representative surface area and particle sizes (Murphy et al., 1976; Janney et al., 2000). The good agreement between the data and the calculation suggests that the mineral core of Fh has an average composition close to FeOOH ($M = 89$ g/mol). This agrees with the standard model that has structural elements

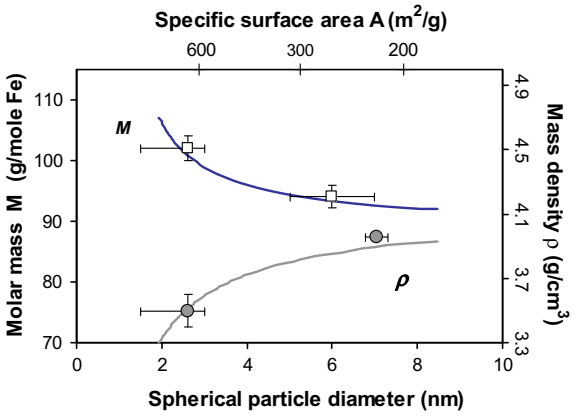

Fig. 5. The calculated relationship between the molar mass M, mass density ρ, particle size d, and specific surface area A of nano-Fh particles. The molar mass (dark blue line, left vertical axis) decreases with increasing particle size (lower horizontal axis) and decreasing surface area (upper horizontal axis). The corresponding mass density (gray line, right vertical axis) increases with particle size. The lines for the molar mass have been calculated assuming FeOOH as the composition of the mineral core and using estimated site densities for the singly- and doubly-coordinated surface groups of 6 nm^{-2} each. The mass density of the mineral core was estimated using the average molar volume V_O of oxide minerals (Fig. 6). The squares represent the experimental molar mass (Rancourt and Meunier, 2008) of 2L-Fh (left) and 6L-Fh (right), which have a characteristic particle size of 1.5–3 nm and 5–6 nm, respectively (Janney et al., 2000; Murphy et al., 1976). The spheres refer to the experimental mass densities of 2L-Fh (Murphy et al., 1975, 1976) and 6L-Fh (Towe and Bradley, 1967), and both are plotted against the reported particle sizes. (For interpretation of the references to color in this figure legend, the reader is referred to the web version of this paper.)

of α-, γ-, and δ-FeOOH. The greater molar mass of the nanoparticles can be explained by the additional mass of OH/OH_2-containing surface groups, which complete the primary coordination shell of surface Fe rather than being attributed to physisorbed water as has been suggested previously in the literature (Manceau and Gates, 1997).

2.9. Mass density

A larger number of OH and OH_2 per Fe (i.e. a higher molar mass) will lead to a reduction in the overall mass density ρ (g/cm^3). It can be shown (Fig. 6) that for minerals like MgO, $Al(OH)_3$, SiO_2, FeOOH, Fe_2O_3, and others, the average molar volume of the (hydr)oxides is $V_O = 10.8 \pm 0.3\ cm^3$/mol oxygen. This number can be combined with the average number of oxygens per metal ion available in the nanoparticles (n) that can be calculated from $n = n_O + (M_{nano} - M_{core})/M_{H_2O}$ in which n_O is the number of oxygens per metal ion in the mineral core ($n_O = 2$), resulting in $n = 2.7$ for 2-line Fh. The combination of n and V_O leads to the estimated molar volume for 2-line Fh that can also be expressed per mole Fe, giving $V = nV_O = 28.6 \pm 0.8\ cm^3$/mol Fe. Using this value in combination with the calculated molar mass M_{nano} (Eq. (8)) results in an estimated mass density for 2-line ferrihydrite

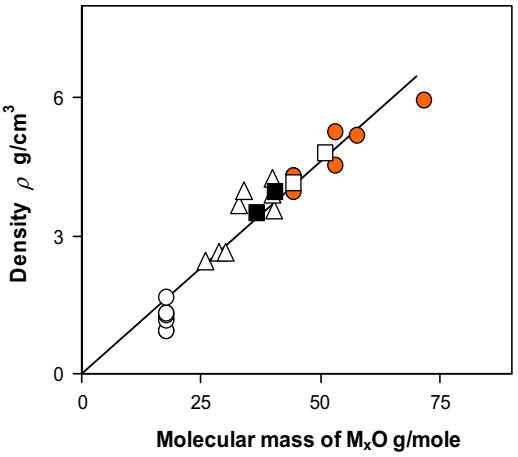

Fig. 6. The mass density ρ (g/cm^3) of minerals versus its molar mass expressed per mole oxygen in the structure for a series of minerals. The open circles are for a number of ice structures, known as ice I–VII. In order of increasing density, the open triangles are for gibbsite, kaolinite, quartz, periclase, corundum, anatase, and rutile. Similarly, the colored spheres refer to the Fe (hydr)oxides: lepidocrocite (γ-FeOOH), goethite (α-FeOOH), feroxyhyte (δ-FeOOH), maghemite (γ-Fe_2O_3), magnetite (Fe_3O_4), hematite (α-Fe_2O_3), and wüstite (FeO). The black squares represent the experimental data for, respectively, 2-line and 6-line ferrihydrites. The open squares refer to, respectively, the core of ferrihydrite as derived in this study and the theoretical value for the recently proposed Fh structure. The inverse value of the slope of the line refers to the average volume of the minerals expressed per mole oxygen, i.e. 10.8 cm^3/mol O. The value is rather constant illustrating that oxygen forms volumetrically the backbone (~90%) of these minerals and of the earth crust in general. (For interpretation of the references to color in this figure legend, the reader is referred to the web version of this paper.)

(2L-Fh) of $\rho = M_{nano}/V = 3.5 \pm 0.1$ g/cm^3. In general, the mass density ρ as a function of the specific surface area A or particle diameter d can be calculated with, respectively:

$$\rho_{nano} = \frac{M_{nano}}{nV_O} = \frac{M_{core}}{n_O V_O} \frac{1}{1 + \left(\frac{M_{core}}{n_O} - M_{H_2O}\right)\frac{N_{H_2O}A}{N_{av}}} \quad (9a)$$

and

$$\rho_{nano} = \frac{M_{nano}}{nV_O} = \frac{M_{core}}{n_O V_O} - \left(\frac{M_{core}}{n_O} - M_{H_2O}\right)\frac{N_{H_2O}}{N_{av}}\frac{6}{d} \quad (9b)$$

in which ρ can be expressed in g/m^3, M_{core} and M_{nano} in g/mol, V_O in m^3/mol oxygen, n_O in mol oxygen/mol metal ion, N_{H_2O} in m^{-2}, A in m^2/g, d in m, and N_{av} in mol^{-1}. The mass density relationship in Fig. 5 has been calculated with Eq. (9) using the above-estimated value V_O for the mineral volume expressed per oxygen (Fig. 6). It is important to note that the molar mass of the core (M_{core}) in Eqs. (8) and (9) will control the vertical positions of the lines in Fig. 5 while the particle size dependency will be predominantly determined by the site density, N_{H_2O}, of chemisorbed water, i.e. the surface contribution. Moreover, note that the lines have been calculated for a fixed site density, whereas the site density may decrease somewhat if the particles grow.

For the small 2L-Fh particles, the impact of the surface is high and a relatively large fraction of all iron will be exposed at the surface (Manceau and Gates, 1997; Poulson et al., 2005). An increase in the particle size will decrease this influence and the mass density of the nanoparticles will ultimately approach the value of the mineral core. In the calculations, this leads to $\rho = 4.15 \pm 0.1$ g/cm^3 for the mineral core when using a single value (no relaxation) for the mineral volume expressed per oxygen ($V_O = 10.8 \pm 0.3$ cm^3/mol oxygen, as derived from Fig. 6). This calculated mass density ρ is between the mass density of lepidocrocite ($\rho = 4.00$ g/cm^3) and goethite ($\rho = 4.26$ g/cm^3) or feroxyhyte ($\rho = 4.29$ g/cm^3).

The predicted mass density, ρ (line), can be compared with experimental observations (Fig. 5). For 2-line ferrihydrite with a particle size of 1.5–3 nm (surface area weighted average 2.6 nm), the reported mass density is 3.5 ± 0.1 g/cm^3 (Murphy et al., 1975, 1976), which is within the error equal to the predicted value. For 6-line ferrihydrite, the reported density is 3.96 g/cm^3 (Towe and Bradley, 1967). The average particle diameter of this Fh preparation can be deduced from the reported molar mass of 200,000–250,000 g/mol particles and gives $d = 7.0 \pm 0.3$ nm. Both mass densities (ρ) have been given in Fig. 5. Data (spheres) and theory (line) match. Note that the overall mass density of 2- and 6-line Fh in relation to the molar mass has been given in Fig. 6 as black squares. In addition, with open squares, the theoretical density of the mineral core derived above is given (4.15 g/cm^3) and the theoretical density (4.8 g/cm^3) of the recently proposed Fh structure. In Fig. 6, the nano particles are at the lower end of the range of Fe (hydr)oxides.

3. DISCUSSION

The above approach for deriving a consistent relationship between properties such as surface site densities and molar mass can in principle be used for other nanoparticles such as anatase (TiO_2). At the surface of anatase, singly- ($\equiv TiOH^{-1/3}$) and doubly-coordinated ($\equiv Ti_2O^{-2/3}$) surface groups are found in a 1:1 ratio with a site density of $N_s = 5.2$–7.0 nm^{-2} for each site depending on the type of crystal face involved (Hiemstra et al., 1996). For nanoparticles with a surface area of 310 ± 10 m^2/g (Ridley et al., 2006), the amount of chemisorbed water is calculated to be about $5.3 \pm 0.5\%$ (Eq. (7)). This number can be compared with the water content measured by thermogravimetric analysis. Water is released from this commercial nano-anatase by two processes. Above about 100 °C, the rate of water release becomes constant. If this process is considered to be due to the release of chemisorbed water, the water content that is released by this process will be ~4% (g/g original sample). This is slightly lower than the estimated value but the dehydroxylation is probably still incomplete at 300 °C. The additional release of physisorbed water below 100 °C was also about 4% (g/g). This loosely bound water is physically adsorbed and may be present partly in the pore space and may be released by outgassing (Navrotsky, 2007). If it is possible to differentiate between physisorbed and chemisorbed water, then the observed

water content can be used to constrain the estimated site density of such nanoparticles.

In the above analysis for Fh, we have not found evidence for a significant contribution of physisorbed water. This may be correct if the samples have been freeze-dried or outgassed before the analysis. IR spectroscopy for Fh has shown that physisorbed water is removed by evacuation at room temperature (Russell, 1979). Without noticeable changes in the BET surface area and the X-ray diffraction pattern, the temperature of repeated outgassing can be raised to a maximum of about 135 °C (Weidler, 1997). The extra amount of water that is released is about 0.13 ± 0.02 g/g 2L-Fh and equal to the estimate given in Section 2.8. This strongly suggests that this water is chemisorbed resulting in the calculated molar mass for 2L-Fh of $M_{nano} = 101 \pm 2$ g/mol Fe. We note that for a freeze-dried 2L-Fh sample a molar mass of 100 g/mol has been reported recently (Mikutta et al., 2008).

The theoretical molar mass of the recently proposed idealized Fh structure (Michel et al., 2007) is significantly lower ($M = 82$ g/mol Fe) and is close to that of hematite ($M = 81$ g/mol Fe), and the proposed structure has a much higher theoretical mass density, i.e. $\rho = 4.9$ g/cm^3 (Rancourt and Meunier, 2008) or $\rho = 4.8$ g/cm^3 (ICSD, 2008) than the experimental and theoretical values for Fh discussed above. Therefore, the recently proposed idealized Fh structure (Michel et al., 2007) is difficult to reconcile with our values unless such particles are severely defect. The deviation is systematic, independent of the particle size and occurs for 2-line as well as 6-line Fh. In both particles, an important part of the Fe^{3+} in the structure has to be replaced by an equivalent amount of H^+ to approach the estimated molar mass and mass density given in Fig. 5. Calculations show that about 20% of the Fe in the structure has to be replaced in the core by an equivalent number of protons (i.e. 0.6 mol H^+ per 0.2 mol Fe). With the standard model, such an assumption is not required. We note that the new structure of Fh contains 20% tetrahedral Fe which so far has not been found by liquid helium Mössbauer spectroscopy as mentioned by Michel et al. (2007).

4. CONCLUSIONS

The above study can be summarized as follows:

- A multisite site complexation (MUSIC) model has been formulated for ferrihydrite. The reactivity of ferrihydrite (Fh) is dominated by the presence of singly-coordinated surface groups. The reactivity of the singly-coordinated surface groups depends on the surface structure. Singly-coordinated surface groups may form the edges of exposed Fe octahedra and provide the sites for the binding of ions such as uranyl and arsenite through the formation of bidentate inner sphere complexes. Other singly-coordinated surface groups, present at a single corner of two adjacent Fe octahedra, may form the sites of double-corner bidentate complexes, which can adsorb ions such as carbonate and phosphate.
- The estimated site density of the singly-coordinated surface groups that form bidentate complexes by double corner or edge sharing coordination is estimated to be $N_s(e) = 2.5 \pm 0.1$ and $N_s(c) = 3.5 \pm 0.4$ nm^{-2}, respectively. In combination with an effective site density for triply-coordinated surface groups ($N_s(tr) = 1.2 \pm 0.2$ nm^{-2}), the overall site density of the proton reactive surface groups of Fh is 7.2 ± 0.7 nm^{-2}. This site density is much greater than the values used in other SCMs that have been derived by the fitting of acid–base titration data. The site density of the doubly-coordinated groups equals the sum of the singly-coordinated ones ($N_s(d) = 6$ nm^{-2}).
- The mineral core of Fh particles has an average chemical composition close to FeOOH and a mass density close to 4.15 ± 0.1 g/cm^3. Theory shows that the molar mass, M, and mass density, ρ, of nano-sized ferrihydrite particles are significantly affected by the contribution of surface groups. Types of sites and corresponding site densities are the essential parameters. For 2.6-nm sized particles (2-line Fh), the enhanced molar mass of the nanoparticles is estimated to be $M \sim 101 \pm 2$ g/mol. The corresponding mass density is reduced to about $\rho \sim 3.5 \pm 0.1$ g/cm^3. The surface area of freshly prepared 2-line Fh is estimated to be approximately $A \sim 650$ m^2/g. A 6-line Fh with a particle size of $d \sim 5$–6 nm, has a surface area of $A \sim 280 \pm 30$ m^2/g, a corresponding molar mass of $\sim 94 \pm 2$ g/mol Fe and a mass density of $\rho \sim 3.9 \pm 0.1$ cm^3/g.
- The PZC of ferrihydrite can be rationalized in terms of the estimated proton affinity constants derived earlier (Venema et al., 1998). As a simplification, one proton affinity constant can be used for all proton reactive surface groups (≡FeOH and ≡Fe_3O). Doubly-coordinated surface groups (≡Fe_2OH) can be considered as non-reactive for the practical pH range.
- The surface charge of nanoparticles generally increases at a decreasing radius. The charging behavior of Fh nanoparticles can be described satisfactory using the flat diffuse double layer (DDL) theory in combination with an enhanced Stern layer capacitance that is particle size dependent, which can be calculated applying spherical condenser theory.

ACKNOWLEDGMENTS

We greatly appreciate the very valuable comments and suggestions of David Kinniburgh. Additionally, the remarks of four other reviewers are gratefully acknowledged, all leading to a substantial improvement of this paper. We also thank the Associate Editor. In addition, we greatly appreciate the theoretical and computational help of Leonard Osté in applying, already many years ago, the spherical double layer theories to nanoparticles.

REFERENCES

Abbas Z., Labbez C., Nordholm S. and Ahlberg E. (2008) Size-dependent surface charging of nanoparticles. *J. Phys. Chem. C* **112**(15), 5715–5723.

Aquino A. J. A., Tunega D., Haberhauer G., Gerzabek M. H. and Lischka H. (2008) Acid–base properties of a goethite surface model: a theoretical view. *Geochim. Cosmochim. Acta* **72**(15), 3587–3602.

Arai Y., Elzinga E. J. and Sparks D. L. (2001) X-ray absorption spectroscopic investigation of arsenite and arsenate adsorption at the aluminum oxide–water interface. *J. Colloid Interface Sci.* **235**, 80–88.

Arai Y. and Sparks D. L. (2001) ATR-FTIR spectroscopic investigation on phosphate adsorption mechanisms at the ferrihydrite–water interface. *J. Colloid Interface Sci.* **241**, 317–326.

Bargar J. R., Kubicki J. D., Reitmeyer R. and Davis J. A. (2005) ATR–FTIR spectroscopic characterization of coexisting carbonate surface complexes on hematite. *Geochim. Cosmochim. Acta* **69**(6), 1527–1542.

Boily J. F., Lützenkirchen J., Balmès O., Beattie J. and Sjöberg S. (2001) Modeling proton binding at the goethite (α-FeOOH)–water interface. *Colloids Surf. A* **179**(1), 11–27.

Burleson D. J. and Penn R. L. (2006) Two-step growth of goethite from ferrihydrite. *Langmuir* **22**(1), 402–409.

Catalano J. G., Park C., Zhang Z. and Fenter P. (2006) Termination and water adsorption at the alpha-Al_2O_3 (0 1 2) – aqueous solution interface. *Langmuir* **22**(10), 4668–4673.

Colombo C., Barrón V. and Torrent J. (1994) Phosphate adsorption and desorption in relation to morphology and crystal properties of synthetic hematites. *Geochim. Cosmochim. Acta* **58**, 1261–1269.

Combes J. M., Manceau A., Calas G. and Bottero J. Y. (1989) Formation of ferric oxides from aqueous-solutions – a polyhedral approach by X-ray absorption-spectroscopy. 1. Hydrolysis and formation of ferric gels. *Geochim. Cosmochim. Acta* **53**(3), 583–594.

Davis J. A. (1977) *Adsorption of Trace Metals and Complexing Ligands at the Oxide/Water Interface*. Stanford University, California, USA.

Davis J. A. and Leckie J. O. (1978) Surface ionization and complexation at the oxide/water interface. II. Surface properties of amorphous iron oxyhydroxide and adsorption of metal ions. *J. Colloid Interface Sci.* **67**, 90–105.

Drits V. A., Sakharov B. A., Salyn A. L. and Manceau A. (1993) Structural model for ferrihydrite. *Clay Miner.* **28**(2), 185–207.

Dzombak D. A. and Morel F. M. M. (1990) *Surface Complexation Modeling: Hydrous Ferric Oxide*. John Wiley & Sons, New York, p. 393.

Eggleston C. M. and Hochella, Jr., M. F. (1992) The structure of hematite {0 0 1} surfaces by scanning tunneling microscopy: image interpretation, surface relaxation, and step structure. *Am. Mineral.* **77**, 911–922.

Evans R. J., Rustad J. R. and Casey W. H. (2008) Calculating geochemical reaction pathways – exploration of the inner-sphere water exchange mechanism in $Al(H_2O)_6^{3+}(aq) + nH_2O$ with ab initio calculations and molecular dynamics. *J. Phys. Chem. A* **112**(17), 4125–4140.

Farquhar M. L., Charnock J. M., Livens F. R. and Vaughan D. J. (2002) Mechanisms of arsenic uptake from aqueous solution by interaction with goethite, lepidocrocite, mackinawite, and pyrite: an X-ray absorption spectroscopy study. *Environ. Sci. Technol.* **36**, 1757–1762.

Felmy A. R. and Rustad J. R. (1998) Molecular statics calculations of proton binding to goethite surfaces: thermodynamic modeling of surface charging and protonation of goethite in aqueous solution. *Geochim. Cosmochim. Acta* **62**, 25–31.

Fenter P. and Sturchio N. C. (2004) Mineral–water interfacial structures revealed by synchrotron X-ray scattering. *Prog. Surf. Sci.* **77**, 171–258.

Gaboriaud F. and Ehrhardt J. (2003) Effects of different crystal faces on the surface charge of colloidal goethite (alpha-FeOOH) particles: an experimental and modeling study. *Geochim. Cosmochim. Acta* **67**(5), 967–983.

Girvin D. C., Ames L. L., Schwab A. P. and McGarrah J. E. (1991) Neptunium adsorption on synthetic amorphous iron oxyhydroxide. *J. Colloid Interface Sci.* **141**, 67–78.

Hiemstra T., De Wit J. C. M. and Van Riemsdijk W. H. (1989) Multisite proton adsorption modeling at the solid/solution interface of (hydr)oxides: a new approach. II. Application to various important (hydr)oxides. *J. Colloid Interface Sci.* **133**, 105–117.

Hiemstra T., Rahnemaie R. and Van Riemsdijk W. H. (2004) Surface complexation of carbonate on goethite: IR spectroscopy, structure and charge distribution. *J. Colloid Interface Sci.* **278**, 282–290.

Van Hiemstra T. and Riemsdijk W. H. (1991) Physical chemical interpretation of primary charging behaviour of metal (hydr)oxides. *Colloids Surf.* **59**, 7–25.

Hiemstra T. and Van Riemsdijk W. H. (1999) Effect of different crystal faces on the experimental interaction force and aggregation of hematite. *Langmuir* **15**(23), 8045–8051.

Hiemstra T. and Van Riemsdijk W. H. (2000) Fluoride adsorption on goethite in relation to different types of surface sites. *J. Colloid Interface Sci.* **225**(1), 94–104.

Hiemstra T. and Van Riemsdijk W. H. (2002) On the relationship between surface structure and ion complexation of oxide–solution interfaces. In *Encyclopaedia of Surface and Colloid Science*. Marcel Dekker, Inc., pp. 3773–3799.

Hiemstra T. and Van Riemsdijk W. H. (2006) On the relationship between charge distribution, surface hydration and the structure of the interface of metal hydroxides. *J. Colloid Interface Sci.* **301**, 1–18.

Hiemstra T., Van Riemsdijk W. H., Rossberg A. and Ulrich K. U. (2009) A surface structural model for ferrihydrite II: adsorption of uranyl and carbonate. *Geochim. Cosmochim. Acta* **73**, 4437–4451.

Hiemstra T., Venema P. and Van Riemsdijk W. H. (1996) Intrinsic proton affinity of reactive surface groups of metal (hydr)oxides: the bond valence principle. *J. Colloid Interface Sci.* **184**, 680–692.

Hsi C.-K. D. and Langmuir D. (1985) Adsorption of uranyl onto ferric oxyhydroxides: application of the surface complexation site-binding model. *Geochim. Cosmochim. Acta* **49**, 1931–1941.

Hwang S. L., Shen P. Y., Chu H. T. and Yui T. F. (2006) A new occurrence and new data on akdalaite, a retrograde mineral from UHP Whiteschist, Kokchetav Massif, Northern Kazakhstan. *Int. Geol. Rev.* **48**(8), 754–764.

ICSD. (2008) *Inorganic Crystal Structure Database*. Fachinformationszentrum FIZ Max-Planck-Society.

Jambor J. L. and Dutrizac J. E. (1998) Occurrence and constitution of natural and synthetic ferrihydrite, a widespread iron oxyhydroxide. *Chem. Rev.* **98**(7), 2549–2585.

Janney D. E., Cowley J. M. and Buseck P. R. (2000) Transmission electron microscopy of synthetic 2-and 6-line ferrihydrite. *Clays Clay Miner.* **48**(1), 111–119.

Janney D. E., Cowley J. M. and Buseck P. R. (2001) Structure of synthetic 6-line ferrihydrite by electron nanodiffraction. *Am. Mineral.* **86**(3), 327–335.

Kim S. W., Seo H. Y., Lee Y. B., Park Y. S. and Kim K. S. (2008) Crystal structure of ferrihydrite nanoparticles synthesized in ferritin. *Bull. Korean Chem. Soc.* **29**(10), 1969–1972.

Koppen S. and Langel W. (2006) Simulation of the interface of (1 0 0) rutile with aqueous ionic solution. *Surf. Sci.* **600**(10), 2040–2050.

Lutzenkirchen J., Boily J. F., Lovgren L. and Sjoberg S. (2002) Limitations of the potentiometric titration technique in determining the proton active site density of goethite surfaces. *Geochim. Cosmochim. Acta* **66**(19), 3389–3396.

Machesky M. L., Wesolowski D. J., Palmer D. A. and Ridley M. K. (2001) On the temperature dependence of intrinsic surface protonation equilibrium constants: an extension of the revised MUSIC model. *J. Colloid Interface Sci.* **239**(2), 314–327.

Majzlan J., Lalinska B., Chovan M., Jurkovic L., Milovska S. and Gottlicher J. (2007) The formation, structure, and ageing of As-rich hydrous ferric oxide at the abandoned Sb deposit Pezinok (Slovakia). *Geochim. Cosmochim. Acta* **71**(17), 4206–4220.

Manceau A. (2009) Evaluation of the structural model for ferrihydrite derived from real space modeling of high-energy X-ray diffraction data. *Clay Miner*. **44**, 19–34.

Manceau A., Charlet L., Boisset M. C., Didier B. and Spadini L. (1992) Sorption and speciation of heavy metals on hydrous Fe and Mn oxides. From microscopic to macroscopic. *Appl. Clay Sci.* **7**, 201–223.

Manceau A. and Gates W. P. (1997) Surface structural model for ferrihydrite. *Clays Clay Miner.* **45**(3), 448–460.

Manceau A., Nagy K. L., Spadini L. and Ragnarsdottir K. V. (2000) Influence of anionic structure of Fe-oxyhydroxides on the structure of Cd surface complexes. *J. Colloid Interface Sci.* **228**, 306–316.

Michel F. M., Ehm L., Antao S. M., Lee P. L., Chupas P. J., Liu G., Strongin D. R., Schoonen M. A. A., Phillips B. L. and Parise J. B. (2007) The structure of ferrihydrite, a nanocrystalline material. *Science* **316**(5832), 1726–1729.

Mikutta C., Mikutta R., Bonneville S., Wagner F., Voegelin A., Christl I. and Kretzschmar R. (2008) Synthetic coprecipitates of exopolysaccharides and ferrihydrite. Part I: characterization. *Geochim. Cosmochim. Acta* **72**(4), 1111–1127.

Murphy P. J., Posner A. M. and Quirk J. P. (1975) Chemistry of iron in soils – ferric hydrolysis products. *Aust. J. Soil Res.* **13**(2), 189–201.

Murphy P. J., Posner A. M. and Quirk J. P. (1976) Characterization of partially neutralized ferric nitrate solutions. *J. Colloid Interface Sci.* **56**(2), 270–283.

Navrotsky A. (2007) Calorimetry of nanoparticles, surfaces, interfaces, thin films, and multilayers. *J. Chem. Thermodyn.* **39**(1), 1–9.

Navrotsky A., Mazeina L. and Majzlan J. (2008) Size-driven structural and thermodynamic complexity in iron oxides. *Science* **319**(5870), 1635–1638.

Ona-Nguema G., Morin G., Juillot F., Calas G. and Brown, Jr., G. E. (2005) EXAFS analysis of arsenite adsorption onto two-line ferrihydrite, hematite, goethite, and lepidocrocite. *Environ. Sci. Technol.* **39**(23), 9147–9155.

Pashley R. M. and Israelachvili J. N. (1984) Molecular layering of water in thin films between mica surfaces and its relation to hydration forces. *J. Colloid Interface Sci.* **101**(2), 511–523.

Ponthieu M., Juillot F., Hiemstra T., van Riemsdijk W. H. and Benedetti M. F. (2006) Metal ion binding to iron oxides. *Geochim. Cosmochim. Acta* **70**(11), 2679–2698.

Poulson R. L., Johnson C. M. and Beard B. L. (2005) Iron isotope exchange kinetics at the nanoparticulate ferrihydrite surface. *Am. Mineral.* **90**(4), 758–763.

Predota M., Bandura A. V., Cummings P. T., Kubicki J. D., Wesolowski D. J., Chialvo A. A. and Machesky M. L. (2004) Electric double layer at the rutile (1 1 0) surface. 1. Structure of surfaces and interfacial water from molecular dynamics by use of ab initio potentials. *J. Phys. Chem. B* **108**(32), 12049–12060.

Rancourt D. G. and Meunier J. F. (2008) Constraints on structural models of ferrihydrite as a nanocrystalline material. *Am. Mineral.* **93**(8–9), 1412–1417.

Ridley M. K., Hackley V. A. and Machesky M. L. (2006) Characterization and surface-reactivity of nanocrystalline anatase in aqueous solutions. *Langmuir* **22**(26), 10972–10982.

Rose J., Manceau A., Masion A. and Bottero J. Y. (1997) Structure and mechanisms of formation of $FeOOH(NO_3)$ oligomers in the early stages of hydrolysis. *Langmuir* **13**(12), 3240–3246.

Rossberg A., Ulrich K. U., Weiss S., Tsushima S., Hiemstra T. and Scheinost A. C. (2009) Identification of uranyl surface complexes on ferrihydrite: advanced EXAFS data analysis and CD-MUSIC modelling. *Environ. Sci. Technol.* **43**(5), 1400–1406.

Russell J. (1979) Infrared spectroscopy of ferrihydrite – evidence for the presence of structural hydroxyl-groups. *Clay Miner.* **14**(2), 109–114.

Rustad J. R. and Felmy A. R. (2005) The influence of edge sites on the development of surface charge on goethite nanoparticles: a molecular dynamics investigation. *Geochim. Cosmochim. Acta* **69**(6), 1405–1411.

Rustad J. R., Felmy A. R. and Hay B. P. (1996) Molecular statics calculations of proton binding to goethite surfaces: a new approach to estimation of stability constants for multisite surface complexation models. *Geochim. Cosmochim. Acta* **60**, 1563–1576.

Schwertmann U. and Taylor R. M. (1989) Iron oxides. In *Minerals in Soil Environments* (eds. J. B. Dixon and S. B. Weed). Soil Science Society of America, pp. 379–438.

Shchukarev A., Boily J. F. and Felmy A. R. (2007) XPS of fast-frozen hematite colloids in NaCl aqueous solutions: I. Evidence for the formation of multiple layers of hydrated sodium and chloride ions induced by the {0 0 1} basal plane. *J. Phys. Chem. C* **111**(49), 18307–18316.

Sherman D. M. and Randall S. R. (2003) Surface complexation of arsenic(V) to iron (hydr)oxides: structural mechanisms from ab initio molecular geometries and EXAFS spectroscopy. *Geochim. Cosmochim. Acta* **67**(22), 4223–4230.

Spadini L., Manceau A., Schindler P. W. and Charlet L. (1994) Structure and stability of Cd^{2+} surface complexes on ferric oxides. 1. Results from EXAFS spectroscopy. *J. Colloid Interface Sci* **168**, 73–86.

Spadini L., Schindler P. W., Charlet L., Manceau A. and Ragnarsdottir K. V. (2003) Hydrous ferric oxide: evaluation of CD-HFO surface complexation models combining Cdk EXAFS data, potentiometric titration results and surface site structures identified from mineralogical knowledge. *J. Colloid Interface Sci.* **266**, 1–18.

Spiccia L. and Casey W. H. (2007) Synthesis of experimental models for molecular inorganic geochemistry – a review with examples. *Geochim. Cosmochim. Acta* **71**(23), 5590–5604.

Sugimoto T. and Wang Y. (1998) Mechanism of the shape and structure control of monodispersed α-Fe_2O_3 particles by sulfate ions. *J. Colloid Interface Sci.* **207**, 137–149.

Sverjensky D. A. (2005) Prediction of surface charge on oxides in salt solutions: revisions for 1:1 (M + L-) electrolytes. *Geochim. Cosmochim. Acta* **69**(2), 225–257.

Tejedor-Tejedor M. I. and Anderson M. A. (1990) Protonation of phosphate on the surface of goethite as studied by CIR-FTIR and electrophoretic mobility. *Langmuir* **6**, 602–611.

Towe K. M. and Bradley W. F. (1967) Mineralogical constitution of colloidal hydrous ferric oxides. *J. Colloid Interface Sci.* **24**(3), 384.

Ulrich K. U., Rossberg A., Foerstendorf H., Zanker H. and Scheinost A. C. (2006) Molecular characterization of uranium(VI) sorption complexes on iron(III)-rich acid mine water colloids. *Geochim. Cosmochim. Acta* **70**(22), 5469–5487.

Venema P., Hiemstra T. and Van Riemsdijk W. H. (1996a) Comparison of different site binding models for cation sorption:

description of pH dependency, salt dependency, and cation-proton exchange. *J. Colloid Interface Sci.* **181**, 45–59.

Venema P., Hiemstra T. and Van Riemsdijk W. H. (1996b) Multisite adsorption of cadmium on goethite. *J. Colloid Interface Sci.* **183**, 515–527.

Venema P., Hiemstra T. and Van Riemsdijk W. H. (1998) Intrinsic proton affinity of reactive surface groups of metal (hydr)oxides: application to iron (hydr) oxides. *J. Colloid Interface Sci.* **198**, 282–295.

Waite T. D., Davis J. A., Payne T. E., Waychunas G. A. and Xu N. (1994) Uranium(VI) adsorption to ferrihydrite: application of a surface complexation model. *Geochim. Cosmochim. Acta* **58**, 5465–5478.

Waychunas G., Trainor T., Eng P., Catalano J., Brown G., Davis J., Rogers J. and Bargar J. (2006) Surface complexation studied via combined grazing-incidence EXAFS and surface diffraction: arsenate on hematite (0 0 0 1) and (1 0 −1 2) (vol 386, pg 2255, 2006). *Anal. Bioanal. Chem.* **386**(7–8), 2255.

Waychunas G. A., Fuller C. C., Rea B. A. and Davids J. A. (1996) Wide angle X-ray scattering (WAXS) study of "two-line" ferrihydrite structure: effect of arsenate sorption and counterion variation and comparison with EXAFS and adsorbed arsenate. *Geochim. Cosmochim. Acta* **60**, 1765–1781.

Waychunas G. A., Rea B. A., Fuller C. C. and Davids J. A. (1993) Surface chemistry of ferrihydrite. 1. EXAFS studies of the geometry of coprecipitated and adsorbed arsenate. *Geochim. Cosmochim. Acta* **57**, 2251–2269.

Weidler P. G. (1997) BET sample pretreatment of synthetic ferrihydrite and its influence on the determination of surface area and porosity. *J. Porous Mat.* **4**(3), 165–169.

Weidler P. G., Hug S. J., Wetche T. P. and Hiemstra T. (1999) Determination of growth rates of 1 0 0 and 1 1 0 faces of synthetic goethite by scanning force microscopy. *Geochim. Cosmochim. Acta* **62**, 3407–3412.

Yamaguchi G., Yanagida H. and Ono S. (1964) A new alumina hydrate, tohdite ($5Al_2O_3 \cdot H_2O$). *Bull. Chem. Soc. Jpn.* **37**(5), 752–754.

Associate editor: Kevin M. Rosso